Results in Physics 10 (2018) 241–247

Contents lists available at ScienceDirect

Results in Physics

journal homepage: www.elsevier.com/locate/rinp

Efficiency enhancement through flat intermediate band in Quantum dot solar cell

Ali Imran[a], Jianliang Jiang[a,*], Deborah Eric[a], Muhammad Noaman Zahid[a], Muhammad Yousaf[b], Muhammad Ahmad[c], Syed Ali Hassan[d]

[a] School of Optics and Photonics, Beijing Institute of Technology, China
[b] Department of Material Science and Engineering, Peking University, China
[c] Department of Structure Engineering, University of Agriculture Faisalabad, Pakistan
[d] Department of Energy Material and Telecommunication, Institut National De La Recherche Scientifique, (INRS), Canada

ARTICLE INFO

Keywords:
Solar cell
Quantum dot
Flat intermediate band
Quantum efficiency
Fermi energy level
Doping concentration

ABSTRACT

Quantum dots (QD) are playing a vital role due to their multifunctionality such as small size and tuning the range of band and have achieved a considerable attention in the recent decade. In recent research, the efficiency of the solar cell (SC) has greatly been increased by application of QD. If these dots are grown systematically, may lead to the formation of the intermediate band (IB) which leads to the absorption of photons with energy less than the actual band through intermediate absorption process and hence increasing the carrier generation rate which ultimately results in high current density keeping the output voltage unaffected. In this paper, we have proposed a method to control the band flatness of the IB in InAs/GaAs QDSC. The flatness is achieved by optimizing the doping concentration and Fermi level (FL) of the surrounding layers. Results show that the maximum 44.12% efficiency can be achieved under maximum optical intensity.

Introduction

The discovery of IBSC has made a breakthrough in the field of modern photovoltaic research. It was first introduced by Marti with the efficiency 63.2% exceeding the previous maximum 33% efficiency proposed by Shockley and Queisser [1,2]. Both of these models were based on detailed balance theory. The detailed balance theory assumes the ideal conditions for the photovoltaic process. However, it is difficult to achieve in practical models due to manufacturing constraints.

An IB can be achieved if QDs are placed in a suitable barrier material with regular symmetry which is referred as QD superlattice [3–7]. The wave functions of closely spaced Quantum dots get coupled and form minibands. These minibands exhibit new optoelectronics properties of this tertiary compound semiconductor which is quite unique from the parent materials [8–13]. This kind of structure may result in the multistep absorption process when sandwiched between the layers of active material. The formation of a new band which is IB provide easier transportation path for the carriers. At the same time, it may also promote the electrons to the conduction band (CB) increasing the overall generation rate [14–22]. There are three possible absorption processes i.e. from valence band (VB) to IB, from IB to CB and from VB to CB. This was impossible in case of single junction SC and only those photons with energies higher than the band gap could be harvested. The higher absorption means higher output current density without voltage degradation. The voltage degradation may occur in case of multi-junction tandem SCs. But in multiband SCs, the IB cannot touch the extraction terminals and hence the output voltage remains equal to the difference of FLs of active material. The high output current and voltage result in higher efficiencies [23–25].

The QD-IBSCs generally contain single intermediate band formed somewhere in the CB offset (CBO) of the barrier and QD material. The theoretically calculated eigen values in case of InAs/GaAs system may have one or two IBs in CBO. But in most cases, it is assumed that there is only one IB [26–31]. This strategy has a great contribution to the efficiency increment of SCs, and many researchers followed the same method. However, there is a very important point needed to be considered that it is not only the CBOs where the carriers are confined but also the VB offset [32–38]. It may also be found in some reports that there is a zero density of states gap between the VB of the active material and the confined VB of QD and barrier system, one of the main reason is that the heavy hole (HH) states may couple with the states of HH in VB of active material. So the FL of IB is supposed to lie inside IB. The ideal condition for the maximum transition through the IB is to dope this region partially and keep it flat. The issue of doping has been

* Corresponding author.
E-mail address: jiangjianliang@bit.edu.cn (J. Jiang).

https://doi.org/10.1016/j.rinp.2018.05.037
Received 27 April 2018; Received in revised form 17 May 2018; Accepted 23 May 2018
Available online 30 May 2018

discussed in many research articles theoretically and experimentally but the band flatness issue has never been addressed [39–45,49–52].

In this article, the detailed balance photovoltaic theory has been applied to calculate the device efficiency. We have proposed a method to control the band flatness of the intermediate band. The two-step absorption phenomena may only take place if there is partially filled flat band in IB layer. In any other case, this layer will not efficiently contribute to second generation process and the output of the device is almost equal to that of normal PIN-SC. The IB flatness is controlled by controlling the doping and the FL of the surrounding layers and a corresponding change in the external quantum efficiencies (QE) are investigated.

Theory and method

The simulation of this model is performed using detailed balance theory which is based on the ideal conditions for the photovoltaic process. The mobilities of the carriers are taken to be constant throughout the device, and each photon with the energy higher than the bandgap energy is supposed to create one electron-hole pair. The back surface is a perfect radiative reflector and both radiative and non-radiative recombination are considered. Finally, each electron-hole pair created in this process is collected at the device terminal. The modeling in case of IBSC is quite complex compared with a single bandgap and single junction SC. The introduction of symmetric arrays of QDs lead to the generation of IB resulting in E_L and E_H, which can be seen in Fig. 1(a). The values of these energies can be found by following equations.

$$E_H = E_{IB} - E_V \tag{1}$$

$$E_L = E_{CB} - E_{IB} \tag{2}$$

$$E_g = E_H + E_L \tag{3}$$

There are three kinds of absorption processes may occur in this case, from VB to IB, IB to CB and VB to CB denoted by α_1, α_2 and α_3 respectively. The relationship between absorption coefficients corresponding to different energies can be seen in Fig. 1(b).

In our work, we have investigated the band flatness controlling through the doping concentration in the surrounding layer of the IB layer. The IB energy level is taken to be 1.05 eV for IB layer made by InGaAs. The Fermi energy level of IB layer is denoted by E_{fIB}. In various studies, it can be noted that this Fermi energy level is supposed to be pinned. To achieve this situation in practical design, the IB layer is required to be doped with suitable donor material which can be found by the following equation.

$$E_{fIB} = E_i + kT \cdot \ln\left(\frac{n_{IB}}{n_{iIB}}\right) \tag{4}$$

where E_i, n_{iIB} and n_{IB} are the intrinsic energy level, intrinsic carrier concentration and a number of electrons in the IB. The intrinsic energy can be found as

$$E_i = \frac{E_g}{2} + kT \cdot \ln\left(\frac{N_C}{N_V}\right) \tag{5}$$

and

$$n_{iIB} = \left(\frac{N_C}{N_V}\right)^{1/2} exp\left(\frac{-E_g}{2kT}\right) \tag{6}$$

where Eg can be deduced from E_{IB}, N_C and N_V effective density of states in CB and VB, where n_{iIB} is the intrinsic carrier concentration in IB. The total number of electrons in the IB can be found as,

$$n_{IB} = n_{iIB} exp\left(\frac{E_{fIB} - E_{IB}}{kT}\right) \tag{7}$$

which is the required number of an electron to achieve the pinning condition for the E_{fIB} and is equal to the doping concentration in case of complete ionization condition. This kind of doping provides partial doping of IB which is very important for the two-step carrier transition, i.e., from VB to IB and from IB to CB. The carrier distribution, in this case, can be found as,

$$n_{IB} = \frac{N_{IB}}{exp\left(\frac{E_{fIB} - E_{IB}}{kT}\right) + 1} \tag{8}$$

where N_{IB} is the number of electron states per unit volume in IB [46,47]. The second and the most important step is the doping of the neighboring layers surrounding the IB layer. The IB can be kept completely flat if the FL of surrounding layer is the same as in IB layer. The required doping concentration, in this case, can be found calculated using above equations. The geometrical structure of IBSC is given in Fig. 2. It can be seen that there is PI layer which gets slightly doped due to the diffusion of holes from neighboring P layer. Similar is the case with IN layer. The values of the parameters used in this modeling are given in Table 1.

Results and discussion

The energy values for the IB with different barrier width of the square-shaped QDs within volume 27 nm^3 are calculated. The simplest case is the two QDs which can be seen in Fig. 3(a) and 4 × 4 QD superlattice in Fig. 3(b). The corresponding wave functions for the ground

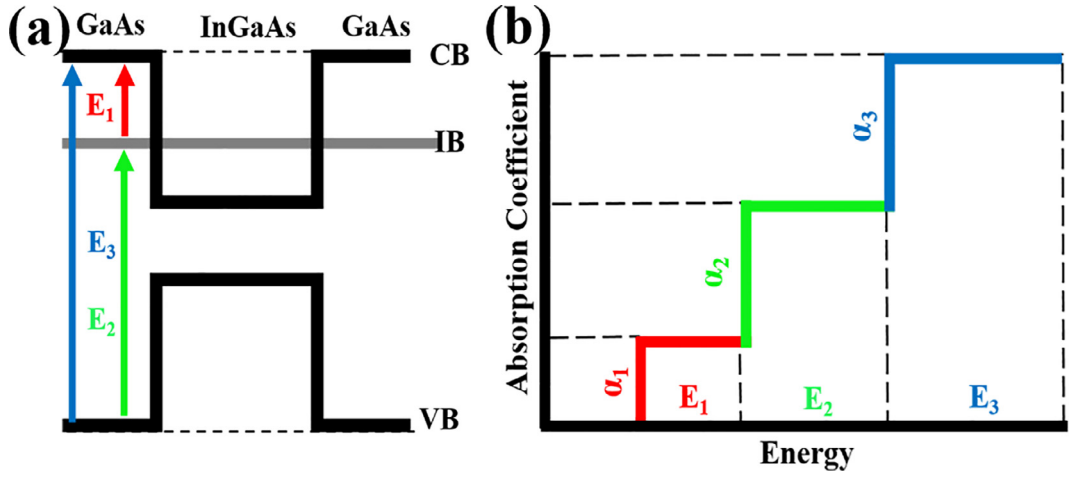

Fig. 1. (a) Schematic of IB formed by QDs (b) Formation of three-step absorption process.

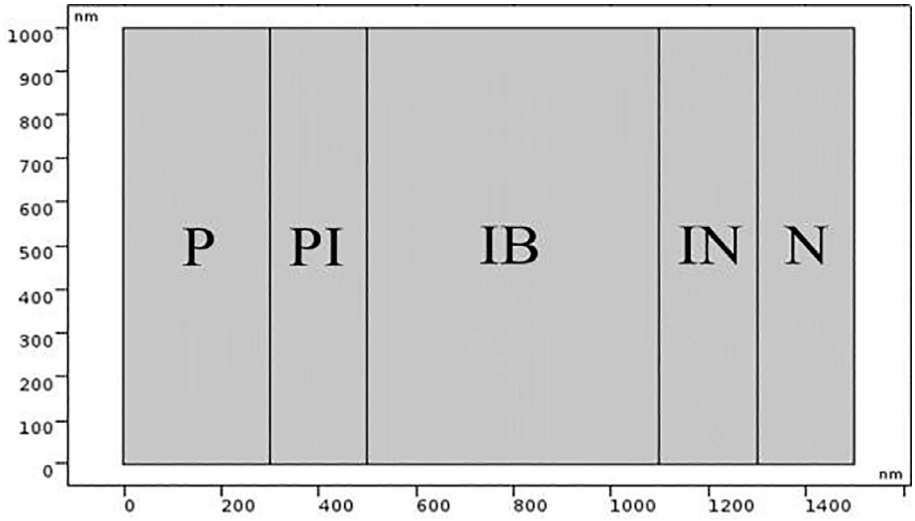

Fig. 2. Geometrical structure of IBSC.

Table 1
Simulation parameters [48,53]

Layer	Thickness (nm)	Doping (cm^{-3})	Electron mobility ($cm^2 V^{-1} s^{-1}$)	Hole mobility ($cm^2 V^{-1} s^{-1}$)	Electron life time (ns)	Hole life time (ns)
P(GaAs)	300	1×10^{18}	1250	278	3	7
PI(GaAs)	200	5×10^{12}	1250	278	3	7
IB(InGaAs)	600	1×10^{17}	2000	2000	10	50
IN(GaAs)	200	5×10^{12}	1250	278	3	7
N(GaAs)	200	1×10^{18}	1250	278	3	7

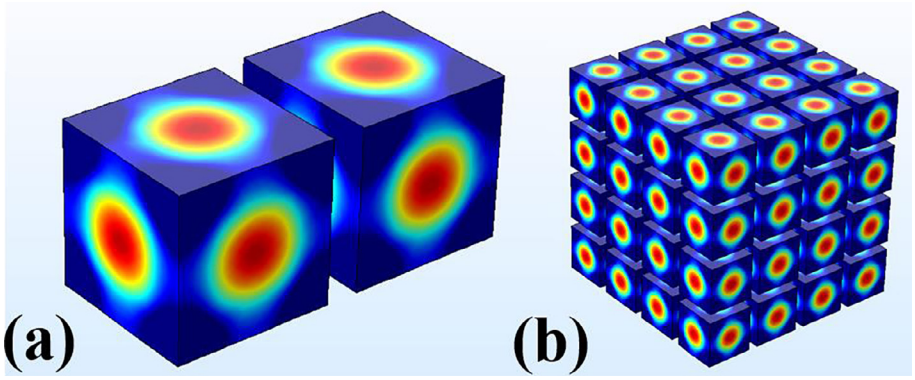

Fig. 3. Simulation of (a) two coupled QDs and (b) 4 × 4 QD superlattice.

state given in Fig. 4(a) and for the excited states in Fig. 4(b). It can be observed that the ground state energy has an inverse relation with the barrier width and minimum energy can be found in case of 2 nm. The ground state energy also depends on the size of QD as well, but we have not calculated that as the focus of this paper is on the doping concentration of intrinsic layers. The probability density of QDs in the ground and excited state is given in Fig. 5. The dependence of the energies on barrier width is given in Table 2.

The optically generated current has been calculated under incident light 1000 Wm^{-2}. The absorption of this light highly depends on the optical properties of the constituent materials. The absorption coefficient depends on the gap energies which has been discussed earlier. The dependence of the real part of the refractive index on incident light can be seen in Fig. 6(a). The imaginary part which is directly related to the absorption coefficient is given in Fig. 6(b). It can be observed that the values of the imaginary part of the refractive index are decreasing with increase in the wavelength of the incident light, which means that the absorption process slows down at higher wavelengths.

The optically generated electric field has been carefully studied and the simulation for this process is performed by setting mesh size to 1/500 for the incident wavelength. The equivalent electric field value contour graph is then generated which can be seen in Fig. 7(a). The blue area shows the maximum value of electric field and decreases while crossing the different layers, creating a maximum number of electron-hole pair at P layer boundary and gives less number of electron while approaching to N layer. The nearly linear decrease in the field along arc length or the cell thickness is given in Fig. 7(b). The reason for the decrease is that more and more radiation is absorbed as it penetrates into the material.

The investigation of donor and acceptor doping concentrations in the constituent layers is very important for the current-voltage and external QE calculations. The electron concentrations in different layers of the IBSC due to doping in the equilibrium condition are given in Fig. 8. It can be seen that maximum electron concentration 10^{18} cm^{-3} is

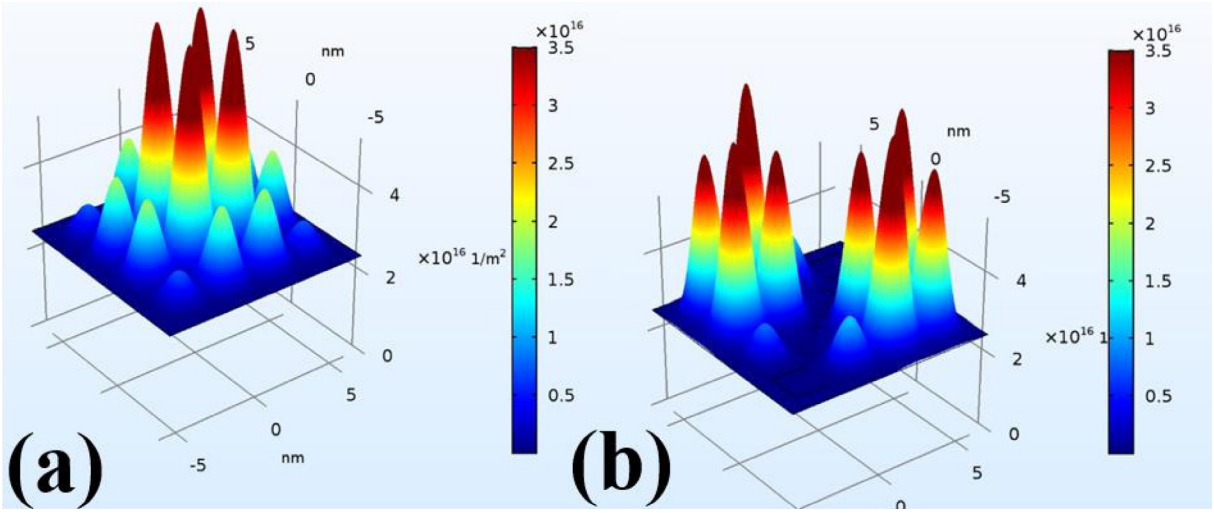

Fig. 4. Height expressions of wave function in (a) Ground state and (b) Excited state.

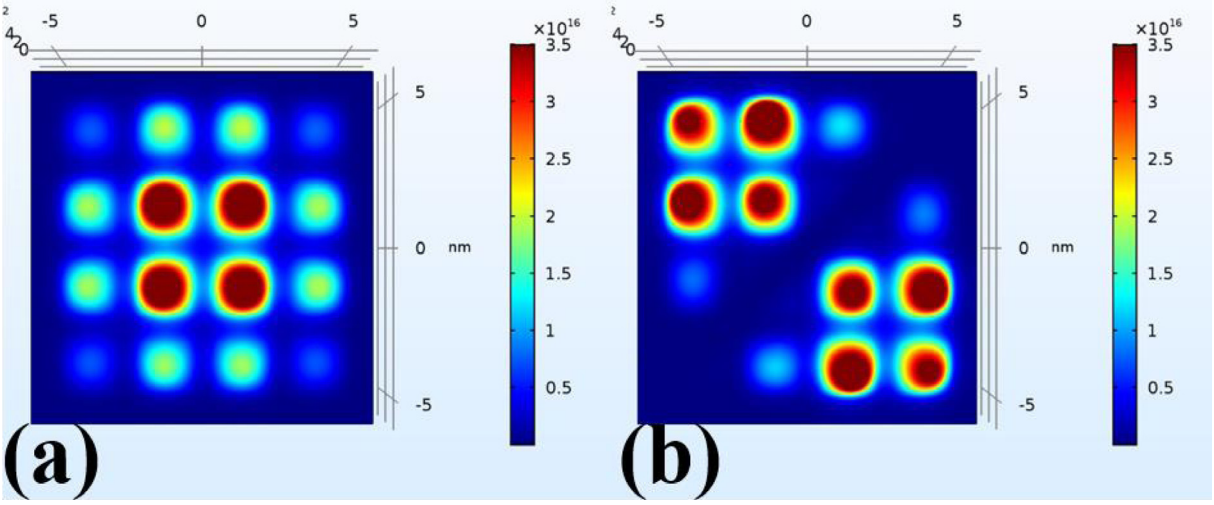

Fig. 5. Vertical views of probability density in (a) Ground state and (b) Excited state.

Table 2
Intermediate Band energies for different barrier width values.

No	QD size (nm)	Barrier Size (nm)	E_{IB} (eV)	E_H (eV)
1	3.00	2.00	0.23	1.19
2	3.00	4.00	0.30	1.12
3	3.00	6.00	0.31	1.11
4	3.00	8.00	0.35	1.07
5	3.00	10.00	0.37	1.05

in the N layer shown by the red color in Fig. 8(a) and (b). Similarly, the doping concentration of the hole in the device has also been investigated under equilibrium condition which can be seen in Fig. 9(a) and (b). The increased numbers of electron and hole in different layers lead to generation of built-in potential, which is maximum at the external boundary of N layer and decreases towards P layer having a minimum value at the external boundary. The potential profile changes while applied under external bias to study the current-voltage characteristics. So the potential decreases under forward voltage and become zero for the maximum output voltage. The value of the maximum output voltage depends on the difference of the FL energies of the P and N layers and the intensity of the incident light [7].

The flat band condition for whole IB region can be achieved if the diffusions of the high carrier concentrations of N layer and P layer are buffered through extra layers, which are PI and IN in our case. Further, the FL of these extra layers must be equalized to the FL of the IB layer through proper doping. The SC is then treated in dark current condition under applied forward bias, where the maximum voltage is taken to be to 1.2 V. Fig. 10 shows the potential profile of the device under an equilibrium condition.

The efficiency of IBSC is investigated under different doping concentrations of PI and IN layers corresponding to the FL of IB, which is supposed to be pinned with IB energy. The Fermi energy level for IB is 1.05 eV in this model. The reason for choosing this value is that this value is achievable in the actual growth process of QD-IB. The required doping concentration for PI and IN layers at FL of 1.05 eV is calculated to be $4.7 \times 10^{18}\,m^{-3}$. The doping concentration is varied for a different range having a maximum value of $5.1 \times 10^{18}\,m^{-3}$. The current-voltage characteristics can be seen in Fig. 11 with a maximum optical intensity of $1000\,Wm^{-2}$. It can be seen that the current density increases with increase in the doping concentration with a very slight change in the output voltage. The increment of the doping concentration beyond $4.7 \times 10^{18}\,m^{-3}$ not only results in higher current value, but also in the lower open-circuit voltage value leading to lower QEs. The maximum efficiency can be observed to be 44.12% with current density to be $457\,Am^{-2}$ at open-circuit voltage of 1.18 V. The current-voltage characteristics of IBSC for different doping concentrations are given in Table 3.

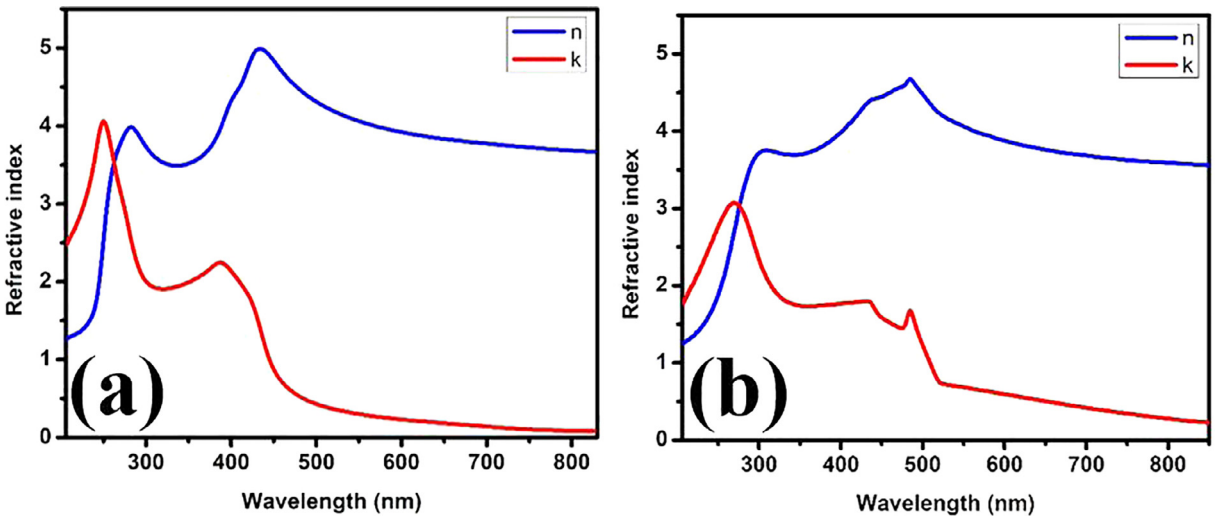

Fig. 6. Refractive index of (a) GaAs and (b) InGaAs.

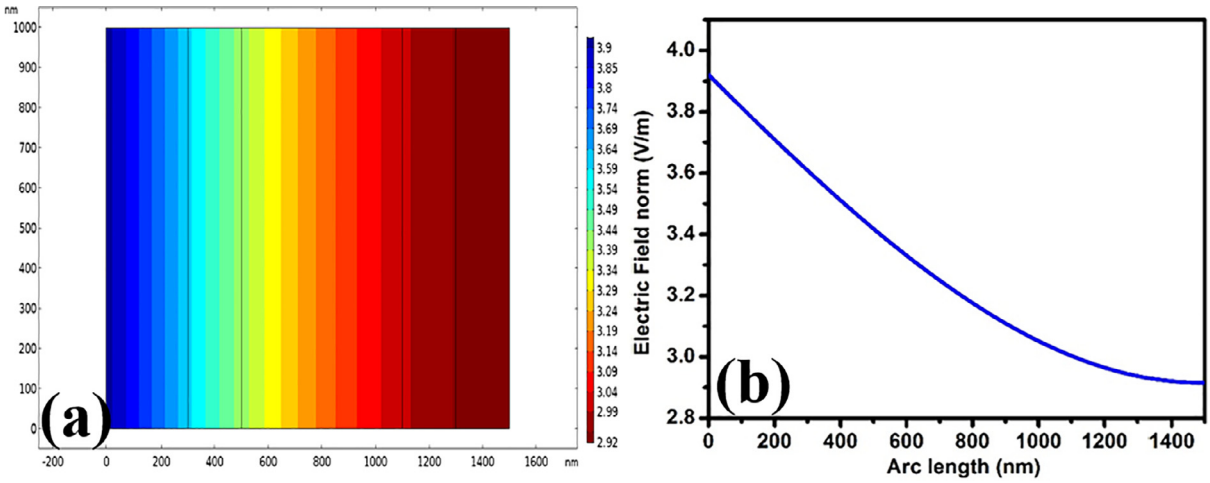

Fig. 7. (a) Surface electric field by incident radiation in 2D (b) Decrease in the electric field along cell thickness.

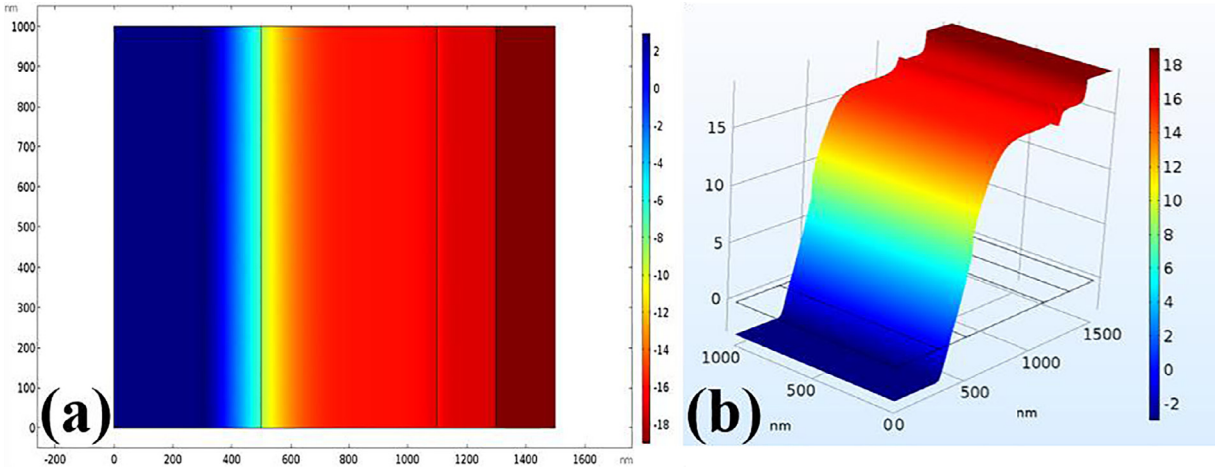

Fig. 8. (a) Electron concentration in 2D (b) Height expression of electron concentration.

Conclusion

In summary, we have investigated the band flatness controlling of the partially doped IB layer. Different values of doping concentration in the intrinsic layers surrounding the IB are applied and corresponding changes in the QE of SC are investigated. Simulation results show that the efficiency of the IBSC highly depends on the flat band region. A decrease in the output voltage is observed at higher values of the doping concentration as the recombination process is higher compared to carrier generation. The maximum efficiency in this research work is

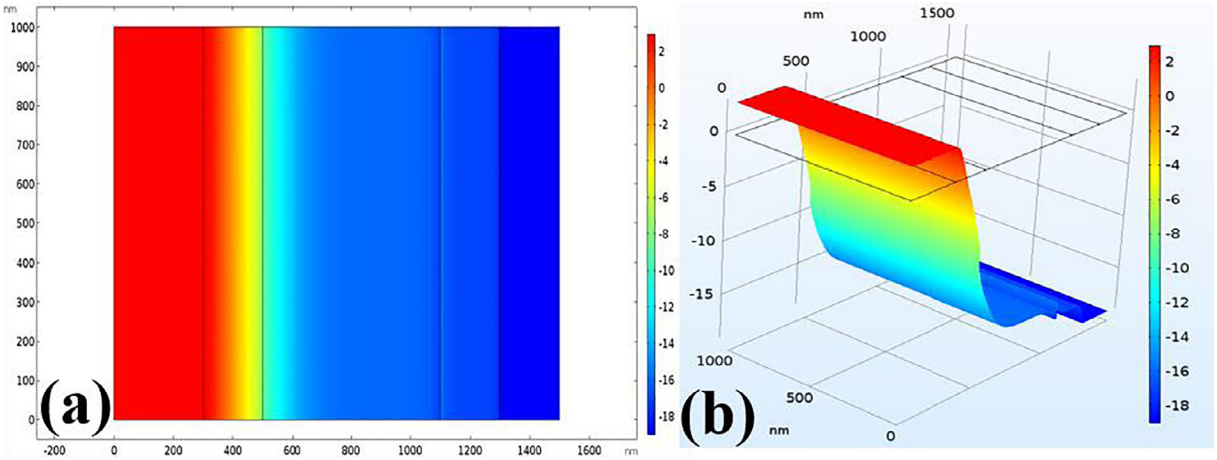

Fig. 9. (a) Hole concentration in 2D (b) Height expression of hole concentration.

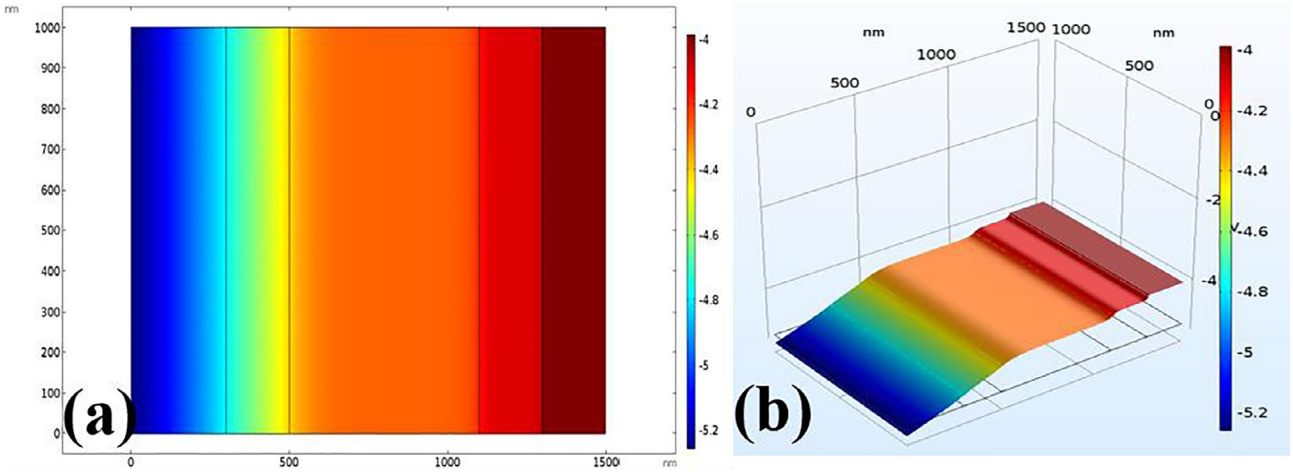

Fig. 10. (a) Electric potential in 2D (b) Height expression of electric potential.

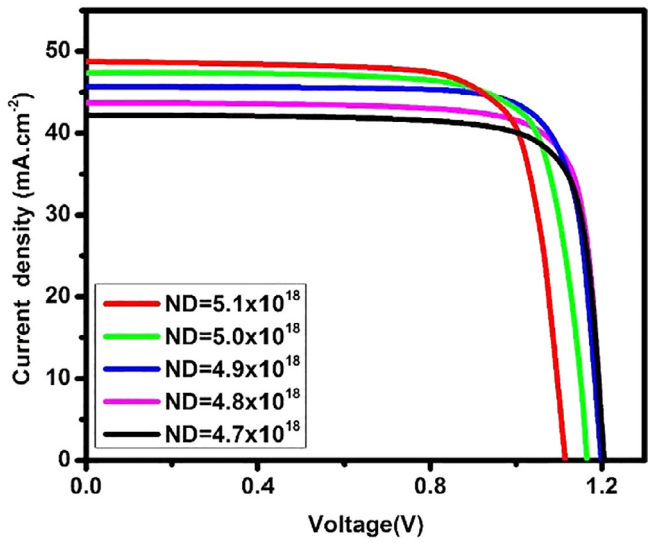

Fig. 11. Current-voltage characteristics of QD-IBSC with different doping concentration ND (m^{-3}).

calculated to be 44.12% at the maximum optical intensity. We have proposed an innovative flat band IBSC structure in this paper which may be fabricated through molecular beam epitaxy, having efficiency much higher compared to the available IBSCs.

Table 3
Current-voltage characteristics of IBSC for different doping concentrations.

No.	Doping Concentration (m^{-3})	Current Density (Am^{-2})	Open Circuit Voltage (V)	Efficiency (%)
1	4.7×10^{18}	422	1.200	39.66
2	4.8×10^{18}	437	1.196	43.16
3	4.9×10^{18}	457	1.184	44.12
4	5.0×10^{18}	473	1.164	42.94
5	5.1×10^{18}	488	1.110	41.84

Appendix A. Supplementary data

Supplementary data associated with this article can be found, in the online version, at http://dx.doi.org/10.1016/j.rinp.2018.05.037.

References

[1] Shockley W, et al. Detailed balance limit of efficiency of p-n junction solar cells. J Appl Phys 1961;32(3):510–9.
[2] Luque A, et al. Increasing the efficiency of ideal solar cells by photon induced transitions at intermediate levels. Phys Rev Lett 1997;78(26):5014–7.
[3] Grenko A. et al. In: Solar energy: new materials and nanostructured devices for high efficiency. SWA4 (Optical Society of America).
[4] Yang X-G, et al. Intermediate-band solar cells based on InAs/GaAs quantum dots. Chin. Phys. Lett. 2011;28(3):038401.
[5] Beattie NS, et al. Quantum engineering of InAs/GaAs quantum dot based intermediate band solar cells. ACS Photonics 2017;4(11):2745–50.
[6] Aly AE-M, et al. Theoretical study of one-intermediate band quantum dot solar cell. Int J Photoenergy 2014;2014:10.

[7] Imran A, et al. Size and shape dependent optical properties of InAs quantum dots. Int Conf Opt Instrum Technol 2018;10622:9.
[8] Imran A, et al. Optical properties of InAs/GaAs quantum dot superlattice structures. Results Phys 2018;9:297–302.
[9] Sugaya T, et al. Miniband formation in InGaAs quantum dot superlattice. Appl Phys Lett 2010;97(4):043112.
[10] Rahman MM. et al. In 2014 IEEE 40th photovoltaic specialist conference (PVSC). p. 1092–1095.
[11] Sugaya T, et al. Tunnel current through a miniband in InGaAs quantum dot superlattice solar cells. Sol Energy Mater Sol Cells 2011;95(10):2920–3.
[12] Imran A, et al. Numerical modelling of high efficiency InAs/GaAs intermediate band solar cell. Int Conf Opt Instrum Technol 2018;10622:12.
[13] Sabeur A. et al. In International conference on optical instruments and technology 2015. p. 10 (SPIE).
[14] Lazarenkova OL, et al. Miniband formation in a quantum dot crystal. J Appl Phys 2001;89(10):5509–15.
[15] Aly AE-MM, et al. Theoretical performance of solar cell based on mini-bands quantum dots. J Appl Phys 2014;115(11):114311.
[16] Kurome A. et al. In: 2011 international meeting for future of electron Devices. p. 114–115.
[17] Tomić S. et al. In: 2013 IEEE 39th photovoltaic specialists conference (PVSC). 0333–0336.
[18] Imran A, et al. Fabrication of screen printed optoelectronic CdS/CdTe device. Int Conf Opt Instrum Technol 2015;9624:8.
[19] Tahir M, et al. Efficient water oxidation through strongly coupled graphitic C3N4 coated cobalt hydroxide nanowires. J Mater Chem A 2016;4:12940–6.
[20] Mahmood N, et al. Control over large-volume changes of lithium battery anodes via active–inactive metal alloy embedded in porous carbon. Nano Energy 2015;15:755–65.
[21] Mahmood N, et al. Electrocatalysts for hydrogen evolution in alkaline electrolytes: mechanisms, challenges, and prospective solutions. Adv Sci 2018;5:1700464.
[22] Jian X, et al. Facile Synthesis of Three-Dimensional Sandwiched MnO2@GCs@MnO2 Hybrid Nanostructured Electrode for Electrochemical Capacitors. ACS Appl Mater Interfaces 2017;9:18872–82.
[23] Hu WG, et al. Effects of absorption coefficients and intermediate-band filling in InAs/GaAs quantum dot solar cells. Appl Phys Lett 2010;97(19):193106.
[24] Levy MY, et al. Intraband absorption in solar cells with an intermediate band. J Appl Phys 2008;104(11):113103.
[25] Luque A, et al. Interband absorption of photons by extended states in intermediate band solar cells. Sol Energy Mater Sol Cells 2013;115:138–44.
[26] Tomić S, et al. Absorption characteristics of intermediate band solar cell. AIP Conf Proc 2010;1199(1):499–500.
[27] Levy MY, et al. Absorption coefficients of intermediate-band media. J Appl Phys 2009;106(7):073103.
[28] Blank B. et al. In: 2014 IEEE 40th photovoltaic specialist conference (PVSC). p. 3457–3462.
[29] Adelhelm R, et al. Performance and parameter analysis of tandem solar cells using measurements at multiple spectral conditions. Sol Energy Mater Sol Cells 1998;50(1):185–95.
[30] Kuo MK, et al. Optical Properties of InAs/GaAs Quantum Dots Grown by Epitaxy. Asme Int Mech Eng Congr & Exposition 2004:549–54.
[31] Gaan S, et al. Size, shape, composition, and electronic properties of InAs/GaAs quantum dots by scanning tunneling microscopy and spectroscopy. J Appl Phys 2010;108(11):114315.
[32] Fry PW, et al. Electronic properties of InAs/GaAs self-assembled quantum dots studied by photocurrent spectroscopy. Phys E 2001;9(1):106–13.
[33] Liu Y, et al. Electronic coupling in nanoscale InAs/GaAs quantum dot pairs separated by a thin Ga(Al)As spacer. Nanoscale Res Lett 2015;10(1):271.
[34] Saïdi I, et al. Electron and hole energy levels in InAs/GaAs quantum dots: size and magnetic field effects. J Appl Phys 2011;109(3):033703.
[35] Rodríguez AL. et al. In: Proceedings of the 8th Spanish conference on electron devices, CDE'2011. p. 1–4.
[36] Ghosh S, et al. Conduction band offset in InAs/GaAs self-organized quantum dots measured by deep level transient spectroscopy. Appl Phys Lett 2000;76(18):2571–3.
[37] Panchak A, et al. The effect of band offsets in quantum dots. Sol Energy Mater Sol Cells 2016;145:180–4.
[38] Gomez-Campos FM. et al. In: 2010 14th International Workshop on Computational Electronics. p. 1–4.
[39] Zieliński M. Valence band offset, strain and shape effects on confined states in self-assembled InAs/InP and InAs/GaAs quantum dots. J Phys: Condens Matter 2013;25(46):465301.
[40] Mielnik-Pyszczorski A, et al. Limited accuracy of conduction band effective mass equations for semiconductor quantum dots. Sci Rep 2018;8(1):2873.
[41] Tomić S. Intermediate-band solar cells: influence of band formation on dynamical processes in InAs/GaAs quantum dot arrays. Phys Rev B 2010;82(19):195321.
[42] Tomić S, et al. In-plane coupling effect on absorption coefficients of InAs/GaAs quantum dots arrays for intermediate band solar cell. Prog Photovoltaics Res Appl 2015;23(5):546–58.
[43] Zhao Z. et al. In: Conference on lasers and electro-optics/quantum electronics and laser science conference and photonic applications systems technologies. JTuA112 (Optical Society of America).
[44] Inoue T, et al. Impurity doping in self-assembled InAs/GaAs quantum dots by selection of growth steps. J Appl Phys 2010;108(6):063524.
[45] Shih-Yen L, et al. Effect of silicon dopant on the performance of InAs/GaAs quantum-dot infrared photodetectors. Jpn J Appl Phys 2004;43(2A):L167.
[46] Yang X, et al. Improved efficiency of InAs/GaAs quantum dots solar cells by Si-doping. Sol Energy Mater Sol Cells 2013;113:144–7.
[47] Yoshida K, et al. Device simulation of intermediate band solar cells: effects of doping and concentration. J Appl Phys 2012;112(8):084510.
[48] Sikder U. et al. In: 2012 7th international conference on electrical and computer engineering. p. 339–342.
[49] Marti A, et al. Partial filling of a quantum dot intermediate band for solar cells. IEEE Trans Electron Devices 2001;48(10):2394–9.
[50] Strandberg R, et al. Photofilling of intermediate bands. J Appl Phys 2009;105(12):124512.
[51] Marti A, et al. Quasi-drift diffusion model for the quantum dot intermediate band solar cell. IEEE Trans Electron Devices 2002;49(9):1632–9.
[52] Vurgaftman I, et al. Band parameters for III–V compound semiconductors and their alloys. J Appl Phys 2001;89(11):5815–75.
[53] Henry CH, et al. Radiative and nonradiative lifetimes in n-type and p-type 1.6μm InGaAs. Electron Lett 1984;20(9):358–9.